

Quantum state transfer with surface plasmons on a metallic nanoparticle array

Changhyoup Lee,¹ Mark Tame,² James Lim¹ and Jinhyoung Lee¹

¹*Department of Physics, Hanyang University, Seoul 133-791, Korea*

²*QOLS, The Blackett Laboratory, Imperial College London, Prince Consort Road, SW7 2BW, United Kingdom*

(Dated: June 3, 2019)

We investigate a periodic array of metallic nanoparticles as a channel for short distance on-chip nanophotonic quantum communication. The transfer of a quantum state, encoded in the form of a single-qubit wavepacket, is studied under ideal conditions. The effects of loss in the metal are then included in order to put the investigation into a more practical setting and quantify the performance of realistic plasmonic nanoparticle arrays as quantum channels. Our study highlights the benefits as well as the drawbacks associated with nanophotonic periodic systems that use surface plasmons in the quantum regime. The techniques introduced in this work and the results obtained from them are aimed at contributing to the study of plasmonic nanostructures for quantum control applications and probing nanoscale optical phenomena.

PACS numbers: 03.67.-a, 03.67.Mn, 42.50.Dv, 03.67.Lx

I. INTRODUCTION

The emerging field of quantum plasmonics is experiencing intense interest from the plasmonics and quantum optics communities at present [1–19]. Integrated quantum systems featuring surface plasmons are beginning to show remarkable potential for their use in quantum control applications, such as quantum information processing [10–12]. Here, novel capabilities in the way the electromagnetic field can be localized [20, 21] and manipulated [22–26] offer the prospect of miniaturization, scalability and strong coherent coupling to single emitter systems that conventional photonics cannot achieve [12–19]. Recent studies have focused on entanglement preservation [1, 2], quadrature-squeezed surface plasmon propagation [3] and the use of surface plasmons as mediators of entanglement between two qubits [4]. With the advancement of nanofabrication techniques, ordered arrays of closely spaced noble metal nanoparticles have been considered for guiding electromagnetic energy via localised surface plasmon (LSP) modes on scales far below the diffraction limit [27, 28]. Here, energy transport in these plasmonic waveguides relies on near-field coupling between surface plasmons of neighbouring particles [29], with the suppression of scattering into the far-field [30–32]. Recently it was shown that an appropriate arrangement of nanoparticles can form passive linear nanoscale optical devices such as beam splitters, phase shifters and crossover splitters [33–35]. Despite this progress in the area of device design, so far there has been no analysis of the effects of loss in these nanoparticle systems in the quantum regime. It is vital to understand the impact of these effects on the performance of such devices before plasmonic systems can be developed as efficient systems for nanophotonic quantum control applications.

In this work, we carry out such an analysis and investigate quantum state transfer with surface plasmons on a metallic nanoparticle array. The transfer of a quantum state, encoded in the form of a single-qubit wavepacket, is studied under ideal conditions. Then, the effects of loss in the metal due to electronic relaxation are considered in order to put our investigation into a more practical setting and quantify the performance of realistic nanoparticle arrays as quantum channels. We find that state transfer can be achieved for small length arrays even

under nonideal conditions and therefore these arrays may act as channels for short distance on-chip nanophotonic quantum communication. Our study highlights the benefits and drawbacks associated with nanophotonic systems that use surface plasmons in the quantum regime. The results of this work should help in the future study and design of more complex plasmonic structures involving emitter systems for quantum control applications and the probing of novel nanoscale optical phenomena.

We start our investigation in the next section by introducing the nanoparticle array model and quantized mathematical description, along with some basic properties of the system dynamics and the performance of state transfer under ideal conditions. Then, in Section III we consider the effects of damping due to losses associated with the electronic response within the metallic nanoparticles. Finally, we summarize our findings in Section V.

II. PHYSICAL SYSTEM AND MODEL

A. The Hamiltonian

We start with a basic description of the physical system considered, with further details regarding the mathematical model and approximations provided later in this section.

We consider the system depicted in Fig. 1 (a), which is presented in a top-down view. Here, a tapered metallic nanowire waveguide on the left hand side focuses light at the end of its tip in the form of a confined surface plasmon field. This field then couples to the adjacent spherical metallic nanoparticle and excites a localised surface plasmon (LSP). The LSP excitation propagates across the array of metallic nanoparticles by near-field coupling and exits via another tapered metallic nanowire waveguide on the right hand side. All metal regions have a frequency dependent permittivity $\epsilon_m(\omega)$ and dielectric regions have static real and positive permittivity ϵ_d . In Fig. 1 (a), in order to give a specific example of the system being studied, we have chosen the radius of the nanoparticles as $R = 25\text{nm}$ and the distance between nanoparticles in the array as $d = 75\text{nm}$. However, the general model we will introduce allows arbitrary values to be chosen for these pa-

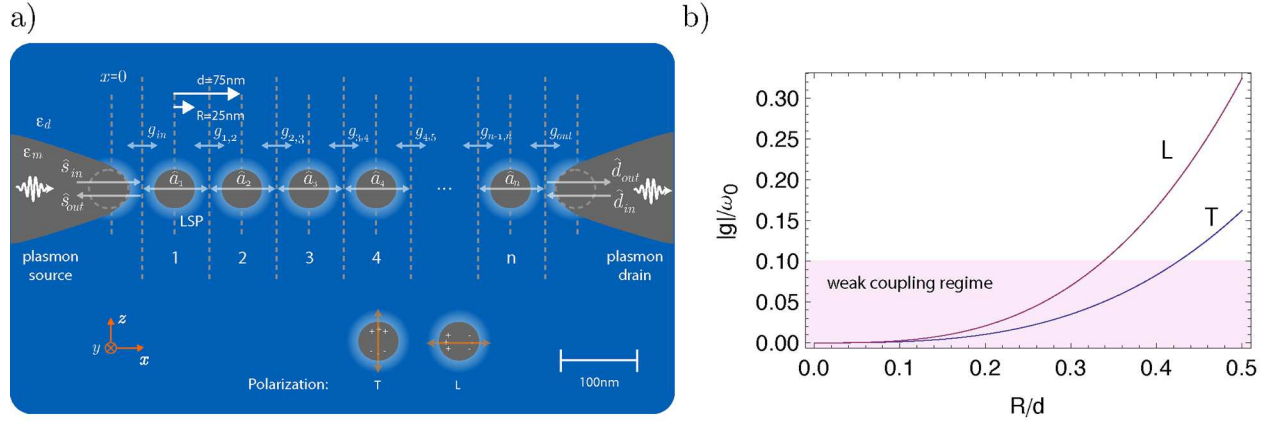


FIG. 1: **(a)**: A tapered metallic nanowire waveguide on the left hand side focuses light to the end of its tip and excites a localised surface plasmon (LSP) on the adjacent nanoparticle. The excitation then propagates across the array of nanoparticles and exits via another tapered metallic nanowire waveguide on the right hand side. All metal regions have permittivity ϵ_m and dielectric regions have permittivity ϵ_d , as defined in the text. The dimensions are chosen as an example and the theory developed is more general, with a range of parameters investigated in this work. **(b)**: Weak coupling approximation for the nanoparticle array. In order to recover the classical dynamics we must work in the regime $|g| \ll \omega_0$ and in particular we choose $\max|g| = 0.1\omega_0$, where ω_0 is the natural frequency of the nanoparticle field oscillations and g is the nearest neighbour coupling parameter. The lower blue curve is for transverse polarization (T) and upper red curve is for longitudinal (L) polarization.

rameters and for all other physical parameters. We consider the metallic nanoparticles in the array support electron charge density oscillations in the Longitudinal (L) and Transverse (T) directions, as shown in the inset of Fig. 1 **(a)** and neglect multipolar interactions [36]. In the system depicted in the main part of the figure, due to the direction in which the electron charge density oscillates in the nanowires, which act as the surface plasmon source and drain on the left and right hand sides, the nanotips at the ends are oriented to excite/collect charge density oscillations in the L direction. For excitation and collection in the T direction, both nanowires should be rotated by 90 degrees either clockwise or anticlockwise.

We now go into the mathematical details and introduce the Hamiltonian for the system, justifying the physical origin of each of the terms appearing. The total Hamiltonian describing the system in Fig. 1 **(a)** is given by

$$\hat{H} = \hat{H}_{np} + \hat{H}_s + \hat{H}_d + \hat{H}_{np,s} + \hat{H}_{np,d}. \quad (1)$$

Here, the first term describes the nanoparticle array system and is given by

$$\hat{H}_{np} = \sum_{i=1}^n \hbar\omega_i \hat{a}_i^\dagger \hat{a}_i + \sum_{[i,j]} \hbar g_{i,j}^p [\hat{a}_i^\dagger \hat{a}_j + \hat{a}_j^\dagger \hat{a}_i], \quad (2)$$

where \hbar is Planck's constant, $[i, j]$ denotes a summation over nearest neighbours j of nanoparticle i , ω_i is the natural frequency of the field oscillation at the i -th nanoparticle, $g_{i,j}^p$ is the coupling strength between the fields of the i -th and j -th nanoparticle, p denotes the direction of oscillation or polarization, $p \in \{L, T\}$, and the operators \hat{a}_i^\dagger (\hat{a}_i) represent the creation (annihilation) operators associated with a field excitation at nanoparticle site i which obey bosonic commutation relations $[\hat{a}_i, \hat{a}_j^\dagger] = \delta_{ij}$. Here we consider a macroscopic quantization of the fields, where the electron response is contained

within the dielectric function of the metal [6, 37]. For the operators, we have suppressed the polarization index p as we will consider surface plasmon dynamics involving only one type of polarization along the array; either $p = L$ or $p = T$ for all operators.

The first term in Eq. (2) represents the free Hamiltonian of the field at the nanoparticles, where ω_i satisfies the Fröhlich criterion, $\text{Re}[\epsilon_m(\omega_i)] = -2\epsilon_d$ [29, 32]. This criterion considers the nanoparticles to be small enough compared to the operating wavelength such that only dipole-active excitations are important [22]. Taking all nanoparticles to have the same permittivity ϵ_m , the local frequencies can be set to be equal, $\omega_i = \omega_0, \forall i$. Due to the spherical symmetry of the nanoparticles, these local frequencies are independent of the polarization. The second term in Eq. (2) represents a nearest-neighbour coupling between the near-field at each nanoparticle. In order to justify the physical mechanism this second term describes and determine how the coupling parameters $g_{i,j}^p$ depend on physical properties of the plasmonic system, we briefly provide the correspondence of the quantum description of the nanoparticle array with the classical description [29].

Consider the state vector $|\psi\rangle = \prod_i |\alpha_i\rangle$, where $|\alpha_i\rangle = e^{-\frac{1}{2}|\alpha_i|^2} e^{\alpha_i \hat{a}_i^\dagger} |0\rangle$ is a coherent state for the i -th site and α_i is the mean field amplitude at this site. Here, the electric field variation of a coherent state $|\alpha\rangle$ approaches that of the classical wave picture in the limit of large field amplitude α [41]. Taking \hat{H}_{np} and $|\psi\rangle$ and substituting them into the Schrödinger equation, $i\hbar \frac{\partial}{\partial t} |\psi\rangle = \hat{H}_{np} |\psi\rangle$, one finds the differential equation for the mean field amplitudes at the sites given as [33]

$$\frac{d\alpha_i}{dt} = -i\omega_0 \alpha_i - i \sum_{[i,j]} g_{i,j}^p \alpha_j. \quad (3)$$

By choosing all the couplings to be equal $g_{i,j}^p = g^p = \frac{1}{2} \frac{\omega_0^2}{\omega_0} \gamma_p$, where $\gamma_T = 1$ and $\gamma_L = -2$ are the relative couplings and

phases for transverse and longitudinal polarization (at a fixed distance, array orientation and nanoparticle size [29]), the differential equation in Eq. (3) is exactly the same as the classical differential equation for the amplitude of the dipole moment p_i associated with the electric field at site i for an array of interacting Hertzian dipoles under the condition $\omega_I \ll \omega_0$ for the interaction frequency ω_I [29, 33]. This is a *weak coupling* approximation and next-nearest neighbour interactions are neglected. In the classical Hertzian model, the dominant interaction in the system is considered to be between the nanoparticle dipoles via the Förster field, which has a $1/d^3$ dependence for $d \ll \lambda$, where $\lambda = \lambda_0/\sqrt{\epsilon_d}$ and λ_0 is the free-space wavelength corresponding to the natural frequency ω_0 of the nanoparticle dipole field [29, 38]. This regime ($d \ll \lambda$) is known as the *near-field* approximation. Furthermore, for $R \lesssim d/3$ the dipoles can be considered point-like [36]. This *point-dipole* approximation is also used in the classical Hertzian model. Thus, by setting $g^p = \frac{1}{2} \frac{\omega_p^2}{\omega_0} \gamma_p$ in the Hamiltonian of the quantum model and ensuring the *weak coupling*, *near-field* and *point-dipole* approximations are satisfied by the physical system, we recover the classical dynamics in the correct limit using coherent states. Here, the interaction frequency is given by $\omega_I = [e^2 \rho_{el} R^3 / 3m^* \epsilon_0 \epsilon_d d^3]^{1/2}$ [29], where e is the electronic charge, ρ_{el} is the electron density of the metal, m^* is the optical effective electron mass and ϵ_0 is the free-space permittivity.

In Fig. 1 (b) we show an example of the dependence of the magnitude of the coupling g (in units of ω_0) as the ratio of R/d increases. Here we have taken the permittivity of the metal $\epsilon_m(\omega)$ as silver and used $\epsilon_m(\omega) = \epsilon_\infty - \omega_p^2/(\omega^2 + i\omega\Gamma) + i/2$, where $\epsilon_\infty = 5$, $\Gamma = 6.25 \times 10^{13}$ rad/s and $\omega_p = 1.402 \times 10^{16}$ rad/s, which are chosen to obtain a best fit to experimental data at frequencies corresponding to freespace wavelengths $\lambda_0 \gtrsim 350$ nm [39], *i.e.* the optical range and above. This leads to $\omega_0 = 5 \times 10^{15}$ rad/s. In addition, we have used $\rho_{el} = 5.85 \times 10^{28} \text{m}^{-3}$, $m^* = 8.7 \times 10^{-31} \text{kg}$ and $\epsilon_d = 1$ [29]. Note that the weak coupling approximation is equivalent to satisfying $|g| \ll \omega_0$ and by imposing $\max|g| = 0.1\omega_0$ one can see from Fig. 1 (b) that for silver for both polarizations we must satisfy $R \lesssim d/3$. This means the point-dipole approximation is immediately satisfied. For the near-field approximation to also be satisfied we require $d \ll 2\pi c/\omega_0 \simeq 377 \text{nm}$. The example in Fig. 1 (a) with $d = 75 \text{nm}$ and $R = 25 \text{nm}$ with silver as the metal satisfies all three of the required approximations.

An additional requirement for the system is that quantum effects other than those due to the quantized surface plasmon field, such as electron tunneling between nanoparticles, are negligible. This puts a lower limit on the distance d between nanoparticles at $\sim 1 \text{nm}$ [40]. However, in order to confidently use the macroscopic approach for the quantization of the surface plasmon field due to the electron response, we assume nanoparticle radii $R \gtrsim 10 \text{nm}$ and therefore $d \gtrsim 30 \text{nm}$. As far as we are aware it is still an open question as to what dimension the macroscopic approach to surface plasmon quantization breaks down. For the moment, in the model we also neglect internal electronic relaxation at each nanoparticle and relaxation of the dipoles into the far-field. We will introduce damping to the system dynamics in the next section.

Continuing with our description of the physical system, the second and third terms of Eq. (1) represent the free Hamiltonian of the surface plasmon fields in the source and drain nanowires on the left and right hand sides of Fig. 1 (a) respectively and are given by

$$\hat{H}_s = \int_{-\infty}^{\infty} d\omega \hbar \omega \hat{s}^\dagger(\omega) \hat{s}(\omega) \quad (4)$$

$$\hat{H}_d = \int_{-\infty}^{\infty} d\omega \hbar \omega \hat{d}^\dagger(\omega) \hat{d}(\omega). \quad (5)$$

The operators of the nanowires correspond to continuum surface plasmon modes which obey the bosonic commutation relations $[\hat{s}(\omega), \hat{s}^\dagger(\omega')] = \delta(\omega - \omega')$ and $[\hat{d}(\omega), \hat{d}^\dagger(\omega')] = \delta(\omega - \omega')$. Again, a macroscopic quantization is carried out for the field [6, 18, 37] and we have extended the integration of ω to cover the range $-\infty$ to ∞ [41].

The surface plasmon excitations in the nanowires are assumed to correspond to the fundamental transverse magnetic (TM) mode with winding number $m = 0$ [18], and can be generated by various methods. For instance, they could be generated via coupling photons from the far-field by focusing the quantized light field onto a grating structure at a thicker part of the tapered nanowire [42]. Another method could be to use end-fire coupling of photons in conventional silica waveguides to the metal nanowires at a much thicker part of the tapered wire [43]. One could even generate the quantized plasmon excitations directly on the wires very close to the tip region by driving emitter systems, such as quantum dots [13] or NV-centers [14], with coherent light to further reduce losses during propagation [18]. Here, the combination of metal and emitter system would provide added flexibility in optimizing the field profile that couples to the nanoparticle - similar to a nanoantenna system [47] - rather than a direct coupling of the emitter system on its own.

The fourth and fifth terms of Eq. (1) represent the coupling of the surface plasmon field of the source nanowire to the LSP field of nanoparticle 1 and the surface plasmon field of the drain nanowire to the LSP field of nanoparticle n respectively. Using a weak-field linearized model [45, 46] the terms are given by

$$\hat{H}_{np,s} = i\hbar \int_{-\infty}^{\infty} d\omega g_{in}(\omega) [\hat{a}_1 \hat{s}^\dagger(\omega) - \hat{s}(\omega) \hat{a}_1^\dagger] \quad (6)$$

$$\hat{H}_{np,d} = i\hbar \int_{-\infty}^{\infty} d\omega g_{out}(\omega) [\hat{a}_n \hat{d}^\dagger(\omega) - \hat{d}(\omega) \hat{a}_n^\dagger]. \quad (7)$$

Here the coupling parameters $g_{in/out}(\omega)$ depend on the strength of the near-field coupling between the nanowires and nanoparticles. Focusing on the case of the source nanowire-to-nanoparticle coupling and considering a propagating surface plasmon in the nanowire entering the region at the nanotip from the left hand side, we have that for an appropriate paraboloidal profile the mode function of the excitation near the tip can strongly couple to a dipole orientated in the direction of the propagation and placed in close proximity [18, 44]. Thus, for the orientation of the source nanotip shown in Fig. 1 (a), the nanowire field couples predominantly to the L polarized oscillation in the nanoparticle. For coupling to the

transverse polarization, the nanotip should be rotated clockwise by 90 degrees. The reciprocal case holds at the drain nanotip and in the orientation shown in Fig. 1 (a), the drain predominantly couples to L polarized field oscillations in the n -th nanoparticle.

Regardless of the excitation method of the plasmons in the nanowire, for a wire that has a slowly varying radius $R(x)$ with distance x along the wire, we have a locally varying dispersion relation given by [48]

$$\frac{\epsilon_m I_1(k_0 \kappa_m R(x))}{\kappa_m I_0(k_0 \kappa_m R(x))} + \frac{\epsilon_d K_1(k_0 \kappa_d R(x))}{\kappa_d K_0(k_0 \kappa_d R(x))} = 0, \quad (8)$$

where I_p and K_p are the modified Bessel functions, $\kappa_m = \sqrt{n^2 - \epsilon_m}$, $\kappa_d = \sqrt{n^2 - \epsilon_d}$, $k_0 = \omega/c$ is the freespace wavenumber at a given frequency ω and $n = n(x, \omega)$ is the local effective refractive index at position x along the nanowire. The radius of the nanotip at the end of the source wire defines the effective radius of the wire in the region just before the tip. We can use this association to determine the approximate dispersion relation of the surface plasmons entering the nanotip region where they couple to the LSP of the first nanoparticle. Therefore, Eq. (8) can be solved for a given set of physical parameters in order to obtain the effective local refractive index $n(x, \omega)$, leading to the dispersion relation $k = n(x, \omega)\omega/c$ for the surface plasmons close to the tip ($x \simeq 0$). In Fig. 2 we show the dispersion relation for a free-space photon $k = \omega/c$, a nanowire surface plasmon (for $R(0) = 25\text{nm}$) using Eq. (8), a standard metal-air interface surface plasmon $k = (\omega/c) \sqrt{\epsilon_m(\omega)/(1 + \epsilon_m(\omega))}$ [6] and the nanoparticle natural oscillation frequency ω_0 . In all cases the example metal is taken to be silver with the dielectric function defined previously. Here we have chosen to represent the wavenumber k in units of an array spacing $d = 75\text{nm}$. Note that only the surface plasmon field from the tip region of a nanowire has the potential to achieve both the correct energy conservation (ω matching) and dipole-coupling [18, 44] for efficient near-field coupling to the first (or last) nanoparticle of the array.

Thus, by setting the coupling g_{in} in $\hat{H}_{np,s}$ according to the physical geometries and tip orientation being considered, one can model coupling of the surface plasmon in the source nanowire to the first nanoparticle and its reflection back along the nanowire. Similarly, by setting the coupling g_{out} in $\hat{H}_{np,d}$, one can model coupling of the last nanoparticle's near-field to the drain nanowire and its reflection back along the nanoparticle array. As the field profiles at the tips are similar in form to those of the nanoparticles, the same physical approximations satisfied by the inter-particle coupling strengths $g_{i,j}$ should be satisfied by the couplings g_{in} and g_{out} in order for the model to be a consistent description. The $g_{\text{in/out}}$ couplings can then be modified to model non-ideal mode function profiles due to the tip shape and other geometrical factors.

B. Input-output formalism

We now wish to use the Hamiltonian in Eq. (1) to model the transmission of a surface plasmon quantum state injected into the array by the source nanowire which then propagates

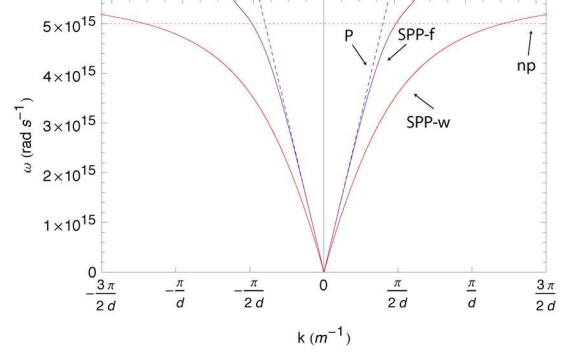


FIG. 2: Dispersion relation for various forms of surface plasmon excitation. Here silver has been chosen as the metal and air as the dielectric background media. The straight dashed line P shows the photon dispersion relation in free-space, the curve SPP-f is the dispersion relation of a surface plasmon field at a standard metal-air interface and the curve SPP-w is the dispersion relation of a surface plasmon field in the tapered metallic waveguide in the region of its tip at a radius of $R = 25\text{nm}$. The horizontal dotted line np is the natural frequency of a single nanoparticle ω_0 . For all curves only the real part of the wavenumber k is plotted. The imaginary part being several orders of magnitude smaller.

along the array until it is subsequently extracted out by the drain nanowire. In order to do this we apply input-output formalism [45, 46] to the system to obtain an effective scattering matrix for the entire process. This scattering matrix will then link the input field operators for the source nanowire to the output field operators for the drain nanowire and provide a method to map arbitrary input quantum states to output quantum states. The benefit of this approach is that we may treat the nanoparticle array as a waveguide with an effective medium, which makes the description of the system in the context of the transfer of quantum states more intuitive. However, it is important to note that one can also use this approach to investigate the internal quantum dynamics of the nanoparticle array and even interactions with other resonant systems, for instance emitter systems such as NV centres, placed in close proximity [45, 46].

We start with the Heisenberg equation of motion for an operator \hat{O} , given by $\frac{d\hat{O}}{dt} = -\frac{i}{\hbar}[\hat{O}, \hat{H}]$ and substitute in the Hamiltonian of Eq. (1) to obtain the equations of motion for each of the system operators

$$\frac{d\hat{s}(\omega)}{dt} = -i\omega\hat{s}(\omega) + g_{\text{in}}(\omega)\hat{a}_1 \quad (9)$$

$$\frac{d\hat{a}_1}{dt} = -\frac{i}{\hbar}[\hat{a}_1, \hat{H}_{np}] - \int_{-\infty}^{\infty} d\omega g_{\text{in}}(\omega)\hat{s}(\omega) \quad (10)$$

$$\frac{d\hat{a}_i}{dt} = -\frac{i}{\hbar}[\hat{a}_i, \hat{H}_{np}], \quad i = 2, \dots, n-1 \quad (11)$$

$$\frac{d\hat{a}_n}{dt} = -\frac{i}{\hbar}[\hat{a}_n, \hat{H}_{np}] - \int_{-\infty}^{\infty} d\omega g_{\text{out}}(\omega)\hat{d}(\omega) \quad (12)$$

$$\frac{d\hat{d}(\omega)}{dt} = -i\omega\hat{d}(\omega) + g_{\text{out}}(\omega)\hat{a}_n. \quad (13)$$

Here we have introduced an explicit time dependence in the frequency space operators $\hat{s}(\omega)$ and $\hat{d}(\omega)$ in the source and

drain respectively. This is because the internal field of the nanoparticle array may acquire some non-trivial dynamics which forces the external fields in the source and drain to have a time dependence that is different from the free field dynamics [45, 46]. With the above set of coupled equations of motion we now find boundary conditions for the system before proceeding to solve them. Using the following solutions for the first and last equations (Eqs. (9) and (13))

$$\begin{aligned}\hat{s}(\omega) &= e^{-i\omega(t-t_0)}\hat{s}_0(\omega) + g_{\text{in}}(\omega) \int_{t_0}^t e^{-i\omega(t-t')} \hat{a}_1(t') dt', \\ \hat{d}(\omega) &= e^{-i\omega(t-t_0)}\hat{d}_0(\omega) + g_{\text{out}}(\omega) \int_{t_0}^t e^{-i\omega(t-t')} \hat{a}_n(t') dt',\end{aligned}$$

where $t_0 < t$, with $\hat{s}_0(\omega)$ and $\hat{d}_0(\omega)$ as the operators for $\hat{s}(\omega)$ and $\hat{d}(\omega)$ respectively at time $t = t_0$ as *initial* boundary conditions, one finds the equations of motion (Eqs. (10) and (12)) for the first and last nanoparticle become

$$\frac{d\hat{a}_1}{dt} = -\frac{i}{\hbar}[\hat{a}_1, \hat{H}_{np}] - \frac{g_{\text{in}}}{2}\hat{a}_1 + \sqrt{g_{\text{in}}}\hat{s}_{\text{in}}, \quad (14)$$

$$\frac{d\hat{a}_n}{dt} = -\frac{i}{\hbar}[\hat{a}_n, \hat{H}_{np}] - \frac{g_{\text{out}}}{2}\hat{a}_n + \sqrt{g_{\text{out}}}\hat{d}_{\text{in}}, \quad (15)$$

where we have defined the input field operators as $\hat{s}_{\text{in}}(t) = -(2\pi)^{-1/2} \int_{-\infty}^{\infty} d\omega e^{-i\omega(t-t_0)} \hat{s}_0(\omega)$ and $\hat{d}_{\text{in}}(t) = -(2\pi)^{-1/2} \int_{-\infty}^{\infty} d\omega e^{-i\omega(t-t_0)} \hat{d}_0(\omega)$. Here we have assumed the couplings $g_{\text{in}}(\omega)$ and $g_{\text{out}}(\omega)$ are constant over a band of frequencies about the characteristic excitation frequency being considered, $g_{\text{in}}^2(\omega) = g_{\text{in}}/2\pi$ and $g_{\text{out}}^2(\omega) = g_{\text{out}}/2\pi$. This assumption is valid for negligible change in the similarity of the modefunction profiles at the tip and nanoparticles over the bandwidth. We assume this can be achieved given a narrow enough band of frequencies along with an optimized nanotip geometry.

Using alternative solutions for the first and last equations of motion

$$\begin{aligned}\hat{s}(\omega) &= e^{-i\omega(t-t_1)}\hat{s}_1(\omega) - g_{\text{in}}(\omega) \int_t^{t_1} e^{-i\omega(t-t')} \hat{a}_1(t') dt', \\ \hat{d}(\omega) &= e^{-i\omega(t-t_1)}\hat{d}_1(\omega) - g_{\text{out}}(\omega) \int_t^{t_1} e^{-i\omega(t-t')} \hat{a}_n(t') dt',\end{aligned}$$

where $t_1 > t$, with $\hat{s}_1(\omega)$ and $\hat{d}_1(\omega)$ as the operators for $\hat{s}(\omega)$ and $\hat{d}(\omega)$ respectively at time $t = t_1$ as *final* boundary conditions, one finds the equations of motion (Eqs. (10) and (12)) for the first and last nanoparticle become

$$\frac{d\hat{a}_1}{dt} = -\frac{i}{\hbar}[\hat{a}_1, \hat{H}_{np}] + \frac{g_{\text{in}}}{2}\hat{a}_1 - \sqrt{g_{\text{in}}}\hat{s}_{\text{out}}, \quad (16)$$

$$\frac{d\hat{a}_n}{dt} = -\frac{i}{\hbar}[\hat{a}_n, \hat{H}_{np}] + \frac{g_{\text{out}}}{2}\hat{a}_n - \sqrt{g_{\text{out}}}\hat{d}_{\text{out}}, \quad (17)$$

where we have defined the input field operators as $\hat{s}_{\text{out}}(t) = (2\pi)^{-1/2} \int_{-\infty}^{\infty} d\omega e^{-i\omega(t-t_1)} \hat{s}_1(\omega)$ and $\hat{d}_{\text{out}}(t) = (2\pi)^{-1/2} \int_{-\infty}^{\infty} d\omega e^{-i\omega(t-t_1)} \hat{d}_1(\omega)$.

Taking Eq. (16) and subtracting Eq. (14) gives the boundary condition

$$\hat{a}_1(t) = \frac{1}{\sqrt{g_{\text{in}}}}(\hat{s}_{\text{in}}(t) + \hat{s}_{\text{out}}(t)). \quad (18)$$

Similarly, taking Eq. (17) and subtracting Eq. (15) gives the boundary condition

$$\hat{a}_n(t) = \frac{1}{\sqrt{g_{\text{out}}}}(\hat{d}_{\text{in}}(t) + \hat{d}_{\text{out}}(t)). \quad (19)$$

Note that throughout we are assuming dispersion is negligible for the initial/final excitations of the source and drain fields. In this sense we are interested only in the relation between the input/output propagating fields in the nanowires near the tips. Dispersion during propagation of the excitations in the nanowires can be incorporated into the model using standard methods [41]. On the other hand, dispersion in the array is included in the model automatically, although we will need to ensure later that minimal broadening of the bandwidth due to dispersion occurs during propagation for the relation $g_{\text{out}}^2(\omega) = g_{\text{out}}/2\pi$ to still hold. We will see that this is a reasonable assumption for small-sized arrays.

Using the relations $[\hat{a}_1, \hat{H}_{np}] = \hbar\omega_1\hat{a}_1 + \hbar g_{1,2}\hat{a}_2$, $[\hat{a}_n, \hat{H}_{np}] = \hbar\omega_n\hat{a}_n + \hbar g_{n-1,n}\hat{a}_{n-1}$ and $[\hat{a}_i, \hat{H}_{np}] = \hbar\omega_i\hat{a}_i + \hbar g_{i-1,i}\hat{a}_{i-1} + \hbar g_{i,i+1}\hat{a}_{i+1}$ (for $i = 2, \dots, n-1$) as well as defining the Fourier components of the nanoparticle field operators as $\hat{a}_i(t) = (2\pi)^{-1/2} \int_{-\infty}^{\infty} e^{-i\omega t} \hat{a}_i(\omega) d\omega$, $\forall i$, and rewriting the source/drain operators as $\hat{s}_{\text{in}}(t) = (2\pi)^{-1/2} \int_{-\infty}^{\infty} e^{-i\omega t} \hat{s}_{\text{in}}(\omega) d\omega$ and $\hat{d}_{\text{in}}(t) = (2\pi)^{-1/2} \int_{-\infty}^{\infty} e^{-i\omega t} \hat{d}_{\text{in}}(\omega) d\omega$ ($\hat{s}_{\text{in}}(\omega)$ and $\hat{d}_{\text{in}}(\omega)$ are general spectral operators), one finds upon substitution into Eqs. (11), (14) and (15) the following set of coupled equations for the frequency operators

$$\begin{aligned}\left[i(\omega - \omega_1) - \frac{g_{\text{in}}}{2}\right] \hat{a}_1(\omega) &= ig_{1,2}\hat{a}_2(\omega) - \sqrt{g_{\text{in}}}\hat{s}_{\text{in}}(\omega) \\ i(\omega - \omega_i)\hat{a}_i(\omega) &= ig_{i-1,i}\hat{a}_{i-1}(\omega) + ig_{i+1,i}\hat{a}_{i+1}(\omega) \\ &\quad \text{for } i = 2, \dots, n-1 \\ \left[i(\omega - \omega_n) - \frac{g_{\text{out}}}{2}\right] \hat{a}_n(\omega) &= ig_{n-1,n}\hat{a}_{n-1}(\omega) - \sqrt{g_{\text{out}}}\hat{d}_{\text{in}}(\omega)\end{aligned}$$

as well as boundary conditions from Eqs. (18) and (19)

$$\begin{aligned}\hat{a}_1(\omega) &= \frac{1}{\sqrt{g_{\text{in}}}}(\hat{s}_{\text{in}}(\omega) + \hat{s}_{\text{out}}(\omega)), \\ \hat{a}_n(\omega) &= \frac{1}{\sqrt{g_{\text{out}}}}(\hat{d}_{\text{in}}(\omega) + \hat{d}_{\text{out}}(\omega)).\end{aligned}$$

Using the above set of coupled equations we can eliminate the internal nanoparticle operators \hat{a}_i [45, 46] to obtain

$$\hat{s}_{\text{in}}(\omega) = \mathcal{R}_s^*(\omega)\hat{s}_{\text{out}}(\omega) + \mathcal{T}_s^*(\omega)\hat{d}_{\text{out}}(\omega), \quad (20)$$

$$\hat{d}_{\text{in}}(\omega) = \mathcal{T}_d^*(\omega)\hat{s}_{\text{out}}(\omega) + \mathcal{R}_d^*(\omega)\hat{d}_{\text{out}}(\omega), \quad (21)$$

where the transmission $\mathcal{T}_{s,d}$ and reflection $\mathcal{R}_{s,d}$ coefficients are functions of the system parameters g_{in} , g_{out} , $g_{i,j}$ and ω_i and the relation $|\mathcal{R}_{s,d}(\omega)|^2 + |\mathcal{T}_{s,d}(\omega)|^2 = 1$. Taking the Hermitian conjugate of Eq. (20) we have $\hat{s}_{\text{in}}^\dagger(\omega) = \mathcal{R}_s(\omega)\hat{s}_{\text{out}}^\dagger(\omega) + \mathcal{T}_s(\omega)\hat{d}_{\text{out}}^\dagger(\omega)$. This allows us to describe the nanoparticle array as an effective waveguide, with transmission $\mathcal{T}_s(\omega) = |\mathcal{T}_s(\omega)|e^{i(k_{np,x}\pm\pi)}$, where $x = (n+1)d$ is the total effective distance (from the centre of the source tip to the centre of the drain tip, as shown in Fig. 1 (a)), the factor $\pm\pi$ takes into account the phase difference of -1 in the definition between the

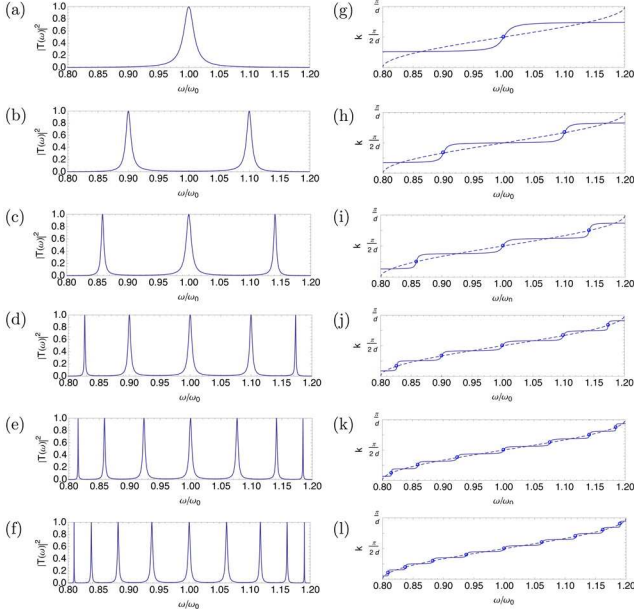


FIG. 3: Transmission spectral profiles and dispersion relations for undamped arrays of nanoparticles. Panels (a)-(f) correspond to the amplitude squared of the transmission, $|\mathcal{T}(\omega)|^2$, as the frequency is varied for an array of $n = 1, 2, 3, 5, 7$ and 9 nanoparticles respectively. Panels (g)-(l) correspond to plots of the effective wavenumber k_{np} for $n = 1, 2, 3, 5, 7$ and 9 respectively. Also shown are points corresponding to the k_{np}^j transmission resonance peaks from panels (a)-(f) as well as the dispersion relation for the infinite array case (dotted line).

input and output field operators and the wavenumber k_{np} depends on the system parameters g_{in} , g_{out} , $g_{i,j}$ and ω_i . We now drop the index s in the transmission coefficient for ease of notation and consider only transmission in the forward direction. Thus we can solve the above set of coupled equations to find $\mathcal{T}(\omega)$ and obtain

$$k_{np} = \frac{\arg(\mathcal{T}(\omega)) \pm \pi \pm 2m\pi}{(n+1)d}, m = 0, \pm 1, \pm 2, \dots \quad (22)$$

where the additional factor of $2m\pi$ is included to reflect the cyclical degeneracy of the wavenumber.

In Fig. 3 (a)-(f) we plot the amplitude squared of the transmission, $|\mathcal{T}(\omega)|^2$, as the frequency is varied for an array of $n = 1, 2, 3, 5, 7$ and 9 nanoparticles respectively. While an analytical form for $\mathcal{T}(\omega)$ can be found, due to the general complexity of all the system parameters, here we show only explicit examples where we have taken all local frequencies to be equal $\omega_i = \omega_0, \forall i$ and the couplings to be equal $g_{i,j} = g_{np} = -0.1\omega_0, \forall i$ and its nearest neighbors j (with the minus sign for the longitudinal polarization, as $\gamma_L = -2$). In Appendix A we provide the analytical form for the $\mathcal{T}(\omega)$'s. Physically, this chosen regime corresponds to an array with $d/R \simeq 3$, for example $R = 25\text{nm}$ and $d = 75\text{nm}$, if we take the metal to be silver as before. The source and drain couplings are set as $g_{in/out} = 0.01\omega_0$, achieved by varying the distance between the nanowire tips and their respective nearest nanoparticle. For a given n , the transmission spectral profiles in Fig. 3 have n resonances at frequencies $\omega_{r_j} = \omega_0 + 2g_{np} \cos(k_{np}^j d)$, where

$k_{np}^j = j\pi/(n+1)d$ for $j = 1, \dots, n$. In Fig. 3 (g)-(l) we plot the effective wavenumber k_{np} from Eq. (22) for $n = 1, 2, 3, 5, 7$ and 9 respectively. Points corresponding to the k_{np}^j transmission resonance peaks from Fig. 3 (a)-(f) are marked. Also included in these figures is the dispersion relation for the infinite array case (dotted line), where the k_{np}^j take on continuous values [33], with a positive group velocity over the entire range due to taking the minus sign (phase) for the longitudinal polarization coupling g in this example. From Fig. 3 (g)-(l) one can clearly see that as the number of nanoparticles n is increased, the band structure of the infinite array case is gradually recovered, where each (ω_{r_j}, k_{np}^j) point corresponds to the dominant excitation of a stationary eigenstate of the system Hamiltonian \hat{H}_{np} , analogous to the case of coupled cavities [49], for instance in the case of photonic crystals [50].

Note that while the above examples provide a very basic insight into the system dynamics, the formalism introduced here can be used to describe more complex and general plasmonic nanoparticle systems with arbitrary couplings and natural local frequencies. We now proceed to focus on odd numbered nanoparticle systems with $n > 1$ in order to understand the transmission properties of larger arrays in more general regimes. A similar study could be made for even numbered systems, however, we choose odd numbered as there is always a resonance at the natural frequency ω_0 . This will become important later in our study of quantum state transfer.

In Fig. 4 (a), (e) and (i) we plot a cross-section of the amplitude squared of the transmission, $|\mathcal{T}(\omega)|^2$, as the frequency ω and couplings $g_{in} = g_{out}$ are varied for an array of $n = 3, 5$ and 7 nanoparticles respectively. Here, $\Delta\omega = \omega - \omega_0$ and we have chosen to plot all parameters in units of the nanoparticle coupling $g_{i,j} = g_{np}, \forall i$ and its nearest neighbors j . The plots are therefore independent of g_{np} , as long as $g_{np} \ll \omega_0$ is satisfied. Increasing (decreasing) g_{np} shrinks (expands) all axes. This observation can be useful when comparing two g_{np} regimes with each other. Note also that $\max(g_{in}/g_{np}^{\max}, g_{out}/g_{np}^{\max}) = 1$ must be imposed, where $g_{np}^{\max} = 0.1\omega_0$, otherwise we move away from the weak coupling regime for the source and drain. In other words, the rescaled couplings g_{in}/g_{np} and g_{out}/g_{np} can go higher than 1, but the value for g_{np} must be lower than $0.1\omega_0$ to compensate so that we are still in the weak coupling regime. In Fig. 4 (b), (f) and (j) we plot a different cross-section for $n = 3, 5$ and 7 nanoparticles, where $g_{in} = 2g_{out}$ and in Fig. 4 (c), (g) and (k) for $g_{in} = g_{out}/2$. In Fig. 4 (d), (h) and (l) we place a threshold on the value of $|\mathcal{T}(\omega)|^2$, with the solid red area corresponding to $|\mathcal{T}(\omega)|^2 \geq 0.98$. One can see that as the source and drain couplings increase, the range over which the transmission is close to ideal becomes enlarged about the central resonance, although if the couplings are too large this range reduces back again. Similar behaviour can be seen for larger odd numbers of nanoparticles, with the central 'fork' area becoming narrower as n increases. This observation will be important in our study of quantum state transfer in the next section.

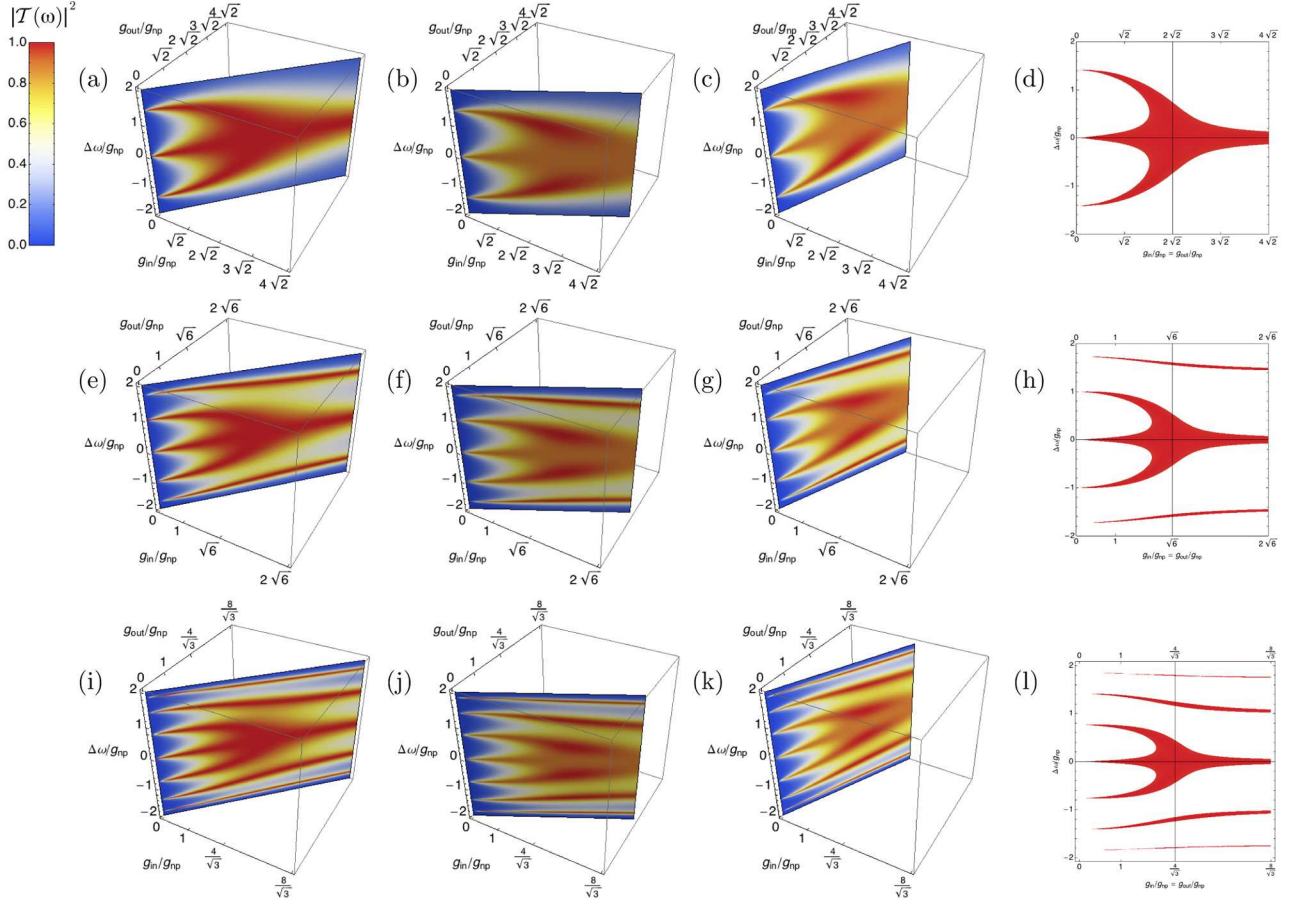


FIG. 4: Cross-sections of the amplitude squared of the transmission, $|\mathcal{T}(\omega)|^2$, as the frequency ω and couplings g_{in} and g_{out} are varied. Panels (a), (e) and (i) correspond to couplings $g_{in} = g_{out}$ for an array of $n = 3, 5$ and 7 nanoparticles respectively. Panels (b), (f) and (j) correspond to $g_{in} = 2g_{out}$ and panels (c), (g) and (k) correspond to $g_{in} = g_{out}/2$. Panels (d), (h) and (l) have a threshold placed on the value of $|\mathcal{T}(\omega)|^2$, with the solid area corresponding to $|\mathcal{T}(\omega)|^2 \geq 0.98$ for $g_{in} = g_{out}$.

C. Example quantum state transfer: Qubit

We now consider the transfer of quantum information in the form of a single quantum bit, or qubit, across a metallic nanoparticle array. We write the input qubit state in the source as $|\psi\rangle_s = \alpha|0\rangle_s + \beta|1_\xi\rangle_s$, where $|1_\xi\rangle_s$ represents a single plasmon wavepacket in the source (at the tip) with a spectral profile $\xi(\omega)$. More explicitly we have

$$|\psi\rangle_s = \alpha|0\rangle_s + \beta \int d\omega \xi(\omega) \hat{s}_{in}^\dagger(\omega) |0\rangle_s. \quad (23)$$

Then for given input state from the source, we take the drain to be initially in the vacuum state $|0\rangle_d$. Using the relation in Eq. (20) and substituting for $\hat{s}_{in}^\dagger(\omega)$, then tracing out the state in the source (see Appendix B), we obtain the output state in the drain nanowire (at the tip) as

$$\begin{aligned} \rho_d = & \left(|\alpha|^2 + |\beta|^2 \int d\omega |\xi(\omega)|^2 (1 - |\mathcal{T}(\omega)|^2) \right) |0\rangle_d \langle 0| \quad (24) \\ & + \alpha\beta^* \int d\omega \xi^*(\omega) \mathcal{T}^*(\omega) |0\rangle_d \langle 1_\omega| \\ & + \alpha^*\beta \int d\omega \xi(\omega) \mathcal{T}(\omega) |1_\omega\rangle_d \langle 0| \end{aligned}$$

$$+ |\beta|^2 \int d\omega \int d\omega' \xi(\omega) \xi^*(\omega') \mathcal{T}(\omega) \mathcal{T}^*(\omega') |1_\omega\rangle_d \langle 1_{\omega'}|$$

where $|1_\omega\rangle_d = \hat{d}_{out}^\dagger(\omega) |0\rangle_d$. For perfect state transfer, *i.e.* $\mathcal{T}(\omega) = e^{i(k_{np}x \pm \pi)}$, giving $|\mathcal{T}(\omega)|^2 = 1$ and $\mathcal{R}(\omega) = 0$, the output state going into the drain nanowire, described by Eq. (24), becomes the pure state $\rho_d = |\psi'\rangle_d \langle \psi'|$, where $|\psi'\rangle_d$ is equivalent to Eq. (23), but with $\xi(\omega) \rightarrow \xi'(\omega) = \xi(\omega)e^{i(k_{np}x \pm \pi)}$ and $\hat{s}_{in}^\dagger(\omega) \rightarrow \hat{d}_{out}^\dagger(\omega)$. The change in the spectral amplitude of the wavepacket is equivalent (upon Fourier transform) to a positive temporal shift (delay) in the wavepacket, which corresponds to the time that the wavepacket takes to move from the source tip to the drain tip. For concreteness, consider a Gaussian wavepacket with spectral amplitude profile

$$\xi(\omega) = (2\pi\sigma^2)^{-1/4} e^{-\frac{(\omega_0 - \omega)^2}{4\sigma^2}}, \quad (25)$$

where ω_0 is the central frequency and $\sigma = \Delta\omega/(2\sqrt{2\ln 2})$ is the standard deviation corresponding to a FWHM bandwidth $\Delta\omega$ for the spectral intensity profile $|\xi(\omega)|^2$. Applying the transform $\xi(\omega) \rightarrow \xi'(\omega) = \xi(\omega)e^{i(k_{np}x \pm \pi)}$ and assuming a small enough $\Delta\omega$ so that there is linear dispersion about ω_0 , then $k_{np} \simeq \omega n_{eff}/c = \omega/c_{eff}$, where n_{eff} and c_{eff} are the effective

refractive index and speed across the nanoparticle array. We can then write $k_{np}x \simeq \omega x/c_{eff} = \omega\delta t$, where δt is the time taken for the wavepacket to propagate from the source tip to the drain tip. Setting $\xi(\omega) \rightarrow \xi'(t) = \pm\xi(\omega)e^{i\omega\delta t}$ and taking the Fourier transform one finds

$$\xi'(t) = \pm(2\sigma^2/\pi)^{1/4} e^{-\sigma^2(t-\delta t)^2 - i\omega_0(t-\delta t)} \equiv \xi(t - \delta t) \quad (26)$$

corresponding to a positive shift, or delay, of δt in the time domain.

We now consider the fidelity of the transfer, defined as $F = \langle \psi' | \rho_d | \psi' \rangle$, where $|\psi'\rangle$ is the ideal transferred state as defined previously. The fidelity describes how close the output state is to the expected one, being zero for orthogonal states and 1 for perfect transfer. Thus we use it to quantify the quality of state transfer. A straightforward substitution gives the more explicit form

$$F = |\alpha|^4 + |\alpha|^2|\beta|^2 \left(\int d\omega |\xi(\omega)|^2 (1 - |\mathcal{T}(\omega)|^2) + 2\text{Re} \left[\int d\omega \xi^*(\omega) \xi'(\omega) \mathcal{T}^*(\omega) \right] \right) + |\beta|^4 \int d\omega \int d\omega' \xi(\omega) \xi'^*(\omega) \xi^*(\omega') \xi'(\omega') \mathcal{T}(\omega) \mathcal{T}^*(\omega'). \quad (27)$$

Using the Bloch sphere coordinates $\alpha = \cos(\theta/2)$ and $\beta = e^{i\phi} \sin(\theta/2)$ and averaging the fidelity $\bar{F} = \frac{1}{4\pi} \int_0^\pi d\theta \int_0^{2\pi} d\phi F \sin\theta$ one finds $|\alpha|^4 \rightarrow 1/3$, $|\beta|^4 \rightarrow 1/3$ and $|\alpha|^2|\beta|^2 \rightarrow 1/6$. Thus, for a given nanoparticle array and input wavepacket defined by $\xi(\omega)$, with a knowledge of $\mathcal{T}(\omega)$ and setting $\xi'(t)$ correctly to the expected profile, one can calculate the average fidelity of the output qubit state going into the drain nanowire using Eq. (27). Note that Eq. (27) is valid for all dispersive regimes, however for simplicity we will limit our discussion to linear dispersion.

In Fig. 5 (a), (c) and (e) we show the average fidelity \bar{F} for an array of $n = 3, 5$ and 7 nanoparticles. Here one can see immediately that for a small enough bandwidth, the state can be transferred across the array with very high fidelity. The dotted red lines correspond to fidelity contours, with the lowest curve (0.66') corresponding to the classical threshold for a quantum channel: the best fidelity achievable by measuring an unknown qubit along a random direction and then sending the result through a classical channel using classical correlations [52]. The solid blue curves correspond to the region in which the dispersion is approximately linear, so that we can use the approximation $k_{np} \simeq \omega n_{eff}/c = \omega/c_{eff}$ to obtain the form of the expected output spectral profile $\xi'(t)$. This region is found by calculating the group velocity $v_G(\omega)$, where $v_G^{-1}(\omega) = \partial k_{np}/\partial \omega'|_{\omega'=\omega}$ and k_{np} is found from Eq. (22). For linear dispersion about the resonant frequency we should have that $v_G(\omega) \simeq v_G(\omega_0)$. In Fig. 5 (b), (d) and (f) we show the scaled group velocity $\tilde{v}_G(\omega) = v_G(\omega)/v_G(\omega_0)$ for an array of $n = 3, 5$ and 7 nanoparticles. One can see that there is a wide frequency range available in the linear dispersive regime, given a large enough input/output coupling can be achieved.

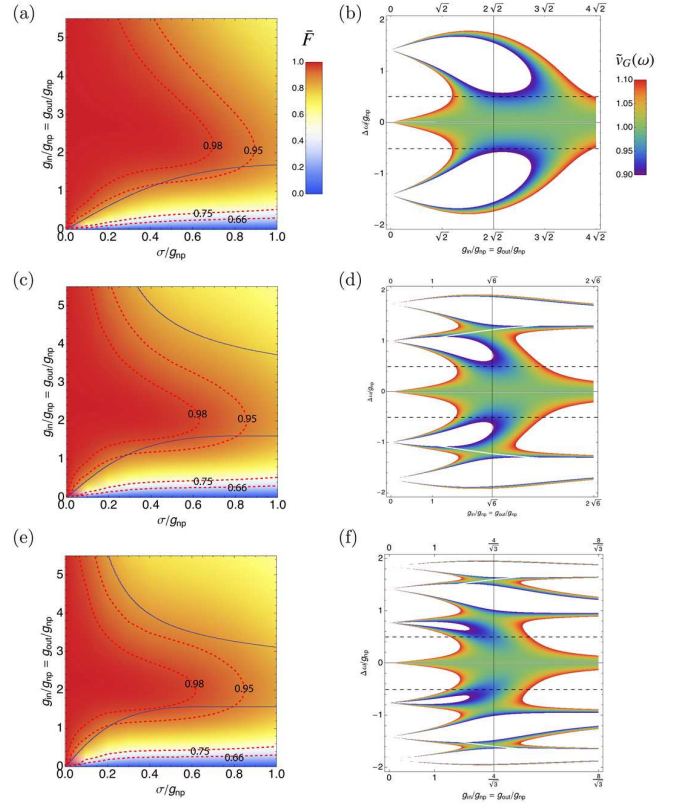


FIG. 5: Fidelity of quantum state transfer for a single qubit wavepacket and scaled group velocity over a range of frequencies and couplings. **(a)**: Average fidelity \bar{F} for transferring a qubit wavepacket over $n = 3$ nanoparticles as the bandwidth (σ) and in/out couplings $g_{in} = g_{out}$ are modified. All parameters are scaled by g_{np} . **(b)**: Scaled group velocity $\tilde{v}_G(\omega) = v_G(\omega)/v_G(\omega_0)$ as it deviates from that at the resonance frequency ω_0 for $n = 3$, showing the regions of approximate linear dispersion. **(c)**: Average fidelity for transferring a qubit wavepacket over $n = 5$ nanoparticles. **(d)**: Scaled group velocity $\tilde{v}_G(\omega)$ as it deviates from that at the resonance frequency ω_0 for $n = 5$. **(e)**: Average fidelity for transferring a qubit wavepacket over $n = 7$ nanoparticles. **(f)**: Scaled group velocity $\tilde{v}_G(\omega)$ as it deviates from that at the resonance frequency ω_0 for $n = 7$. In all group velocity plots, the region inside the dotted lines for $\Delta\omega$ corresponds to the frequency range σ shown in the average fidelity plots.

III. DAMPING

We now include damping in our model. The effects of loss in the system are due to the interaction of the electrons supporting the surface plasmon field with phonons, lattice defects and impurities leading to relaxation [29, 51], as well as radiative scattering of the surface plasmon into the far-field [29]. For most nanoparticle array scenarios the couplings between nanoparticles are large enough such that most of the field remains within the array, with radiative scattering rates generally more than 5 orders of magnitude smaller than the relaxation rate [29], thus we assume that they can be neglected in our model. This assumption also allows us to neglect possible radiative scattering of the field at the tips. Electronic relaxation effects on the other hand cannot be neglected and lead to damping of the supported surface plasmon field. In our model

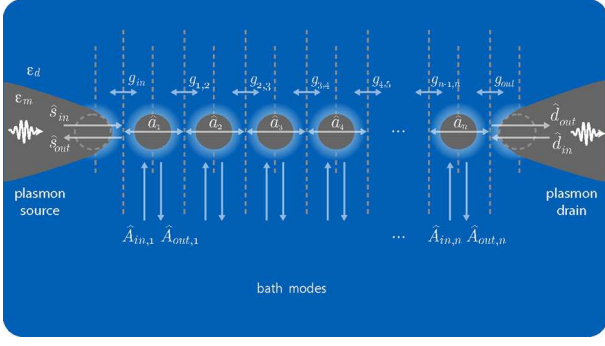


FIG. 6: The plasmonic nanoparticle array including bath modes to model damping at each nanoparticle.

we describe this as an amplitude damping channel acting on the field at each nanoparticle. In this context a mechanism can be introduced where the damping is effectively modeled by coupling of the field at each nanoparticle to separate non-interacting bath modes, which are eventually traced out from the system dynamics, as shown in Fig. 6. As we are interested in the mapping of the input field at the source tip to the output field at the drain tip we assume that the source and drain excitations experience no loss propagating in/out of the tip regions. Such loss can however be incorporated using standard waveguide methods [6, 41], although the specific model will depend on how the fields in the nanowires are excited and collected, for instance, how far they propagate in the nanowires. Various types of dielectric-metal structures can significantly reduce these losses [53].

The interaction of the nanoparticles to their bath modes takes the same form as the coupling of the first nanoparticle to the source nanowire tip, except with a coupling strength determined by the rate of damping chosen to match the classical case, as done previously for the inter-particle couplings $g_{i,j}$. This approach assumes a weak damping rate and Markov approximation for the bath modes [45, 46]. To mathematically incorporate the bath modes into our model, the coupled equations from the previous section are modified to become

$$\begin{aligned} \left[i(\omega - \omega_1) - \frac{g_{\text{in}}}{2} - \frac{\Gamma_1}{2} \right] \hat{a}_1(\omega) &= ig_{1,2}\hat{a}_2(\omega) - \sqrt{g_{\text{in}}}\hat{s}_{\text{in}}(\omega) \\ &\quad - \sqrt{\Gamma_1}\hat{A}_{\text{in},1}(\omega) \\ \left[i(\omega - \omega_i) - \frac{\Gamma_i}{2} \right] \hat{a}_i(\omega) &= ig_{i-1,i}\hat{a}_{i-1}(\omega) + ig_{i+1,i}\hat{a}_{i+1}(\omega) \\ &\quad - \sqrt{\Gamma_i}\hat{A}_{\text{in},i}(\omega), \text{ for } i = 2, \dots, n-1 \\ \left[i(\omega - \omega_n) - \frac{g_{\text{out}}}{2} - \frac{\Gamma_n}{2} \right] \hat{a}_n(\omega) &= ig_{n-1,n}\hat{a}_{n-1}(\omega) \\ &\quad - \sqrt{g_{\text{out}}}\hat{d}_{\text{in}}(\omega) - \sqrt{\Gamma_n}\hat{A}_{\text{in},n}(\omega) \end{aligned}$$

where Γ_i corresponds to the electronic relaxation rate at nanoparticle i . Extra boundary conditions are then imposed on the system dynamics given by

$$\hat{a}_i(\omega) = \frac{1}{\sqrt{\Gamma_i}}(\hat{A}_{\text{in},i}(\omega) + \hat{A}_{\text{out},i}(\omega)), \text{ for } i = 1, \dots, n \quad (28)$$

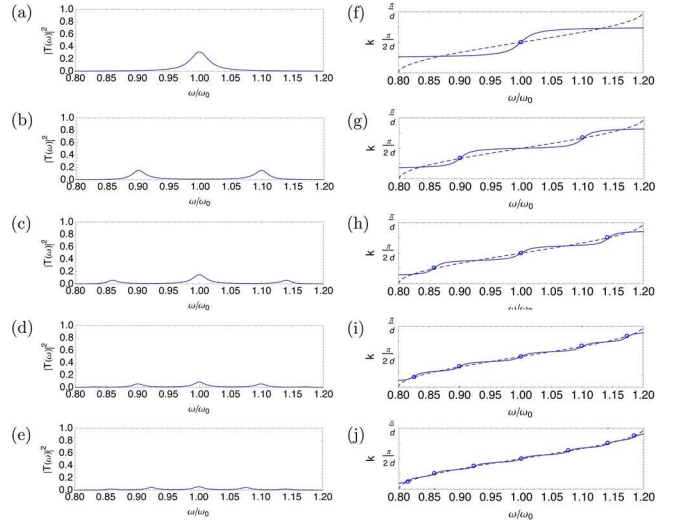


FIG. 7: Transmission spectral profiles and dispersion relations for damped arrays of nanoparticles. Panels (a)-(e) correspond to the amplitude squared of the transmission, $|\mathcal{T}(\omega)|^2$, as the frequency is varied for an array of $n = 1, 2, 3, 5$ and 7 nanoparticles respectively. Panels (f)-(j) correspond to plots of the real part of the effective wavenumber k_{np}^r for $n = 1, 2, 3, 5$ and 7 respectively. Also shown are points corresponding to the $k_{np}^{r,j}$ transmission resonance peaks from panels (a)-(e) as well as the dispersion relation for the infinite array case (dotted line). Here the couplings used are the same as the undamped case, *i.e.* $g_{\text{in}/\text{out}} = 0.01\omega_0$. Note that larger transmission values can be achieved by increasing these couplings, as explained in the text and shown in Fig. 8.

As in the case of the source and drain nanowire system, the bath operators $\hat{A}(\omega)$ obey the bosonic commutation relations $[\hat{A}(\omega), \hat{A}^\dagger(\omega')] = \delta(\omega - \omega')$. By solving the above new set of coupled equations and eliminating the internal nanoparticle operators \hat{a}_i we obtain a scattering matrix linking the source, drain and bath operators. Then for a given input state $|\psi\rangle$ from the source, we take the bath modes (and drain) to be initially in the vacuum state $|0\rangle$. The scattering matrix is applied and the bath modes are traced out to obtain the effective transmission dynamics of the array. In general one finds

$$\hat{s}_{\text{in}}^\dagger(\omega) = \mathcal{R}(\omega)\hat{s}_{\text{out}}^\dagger(\omega) + \sum_i \mathcal{S}_i(\omega)\hat{A}_{\text{out},i}^\dagger(\omega) + \mathcal{T}(\omega)\hat{d}_{\text{out}}^\dagger(\omega), \quad (29)$$

where $|\mathcal{R}(\omega)|^2 + |\mathcal{T}(\omega)|^2 + \sum_i |\mathcal{S}_i(\omega)|^2 = 1$. This method again allows us to describe the nanoparticle array as an effective waveguide, with $\mathcal{T}(\omega) = |\tilde{\mathcal{T}}(\omega)|e^{i(k_{np}x \pm \pi)}$, where $|\tilde{\mathcal{T}}(\omega)|$ is the transmission in the ideal case (no damping) and the wavenumber $k_{np} = k_{np}^r + ik_{np}^i$ has become complex as a result of the damping [41], which now depends on the system parameters $g_{\text{in}}, g_{\text{out}}, g_{i,j}, \omega_i$ and the relaxation rates Γ_i at each nanoparticle. Thus, we have that $|\mathcal{T}(\omega)| = |\tilde{\mathcal{T}}(\omega)|e^{-k_{np}^i x}$. We can then solve the set of coupled equations to find $\mathcal{T}(\omega)$, $\mathcal{R}(\omega)$ and the $\mathcal{S}_i(\omega)$ in order to determine how an arbitrary quantum state is transmitted through the array.

In Fig. 7 (a)-(e) we plot the amplitude squared of the transmission, $|\mathcal{T}(\omega)|^2$, as the frequency is varied for an array of $n = 1, 2, 3, 5$ and 7 nanoparticles respectively. Here, as be-

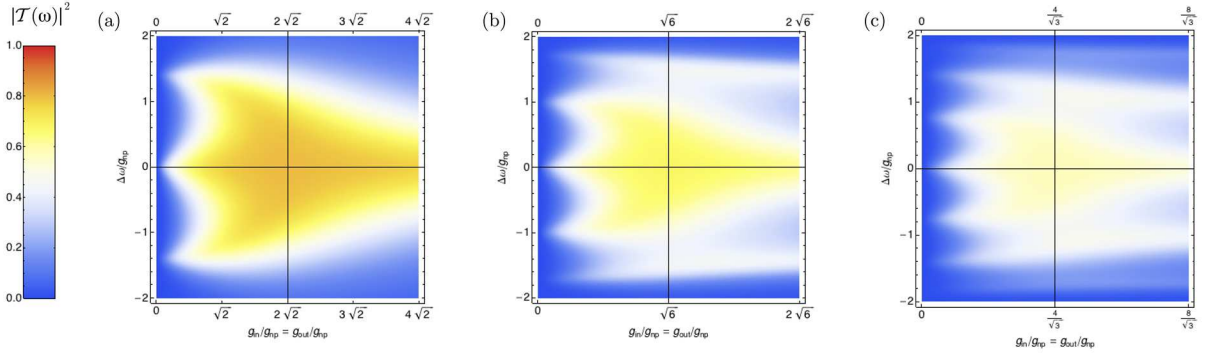


FIG. 8: Damping for the amplitude squared of the transmission, $|\mathcal{T}(\omega)|^2$, as the frequency ω and couplings g_{in} and g_{out} are varied. Panels (a), (b) and (c) correspond to couplings $g_{\text{in}} = g_{\text{out}}$ for an array of $n = 3, 5$ and 7 nanoparticles respectively.

fore we have taken all local frequencies to be equal $\omega_i = \omega_0, \forall i$ and the couplings to be equal $g_{i,j} = g_{np} = -0.1\omega_0, \forall i$ and its nearest neighbors j . In Appendix C we provide the analytical form for the $\mathcal{T}(\omega)$'s. Again, this chosen regime corresponds to an array with $d/R \simeq 3$, for example $R = 25\text{nm}$ and $d = 75\text{nm}$, if we take the metal to be silver. The source and drain couplings are set as $g_{\text{in/out}} = 0.01\omega_0$ to enable a comparison with the ideal case, as shown in Fig. 3. The damping rate for each nanoparticle depends on its size and is given by $\Gamma = v_F/\lambda_B + v_F/R$, where for silver $\lambda_B = 57\text{nm}$ is the bulk mean-free path of an electron and $v_F = 1.38 \times 10^6\text{m/s}$ is the velocity at the Fermi surface [29]. We have used $\Gamma_i = 0.0158\omega_0, \forall i$. This corresponds approximately to the damping rate for a silver nanoparticle with a radius in the range $20 - 100\text{nm}$.

For a given n , the transmission spectral profiles in Fig. 7 again have n resonances at frequencies $\omega_{r_j} = \omega_0 + 2g \cos(k_{np}^{r,j}d)$, where $k_{np}^{r,j} = j\pi/(n+1)d$ for $j = 1, \dots, n$. However, the width of the resonances has been broadened and the height lowered as a result of the damping. In Fig. 7 (f)-(j) we plot the real part of the effective wavenumber $k_{np}^{r,j}$ from Eq. (22) for $n = 1, 2, 3, 5$ and 7 respectively. Note that Eq. (22) remains valid, as the imaginary part is absorbed into the magnitude of the transmission, $|\mathcal{T}(\omega)|$. Points corresponding to the $k_{np}^{r,j}$ transmission resonance peaks from Fig. 7 (a)-(e) are marked. Also included in these figures, as before, is the dispersion relation for the infinite array case (dotted line). From Fig. 7 (g)-(l) one can clearly see that the transmission peaks are much reduced from the ideal values. However, despite this, it is possible to increase the maximum peak value by increasing the source and drain couplings, as shown in Fig. 8 (a), (b) and (c), where we plot a cross-section of the amplitude squared of the transmission, $|\mathcal{T}(\omega)|^2$, as the frequency ω and couplings $g_{\text{in}} = g_{\text{out}}$ are varied for an array of $n = 3, 5$ and 7 nanoparticles respectively. Here, $\Delta\omega = \omega - \omega_0$ and as before, all parameters are in units of the nanoparticle coupling $g_{i,j} = g_{np}, \forall i$ and its nearest neighbors j . One can see from Fig. 8 that as the source and drain couplings (g_{in} and g_{out}) increase, the transmission maximum can be increased, although ultimately the damping dominates the transmission as n increases, as can be seen by comparing Fig. 8 (a) with (c).

We now discuss the fidelity of state transfer for a single

qubit wavepacket state under realistic conditions of loss at each of the nanoparticles. After including the bath modes at each of the nanoparticles, one finds that the expression for the average fidelity given in Eq. (27) remains valid (see Appendix B), with the fidelity depending only on the transmission. In Fig. 9 (a), (c) and (e) we show the average fidelity \bar{F} for an array of $n = 3, 5$ and 7 nanoparticles. The dotted red lines correspond to fidelity contours with the lowest curve (0.66) corresponding to the classical threshold for a quantum channel, as before. The solid blue curves correspond to the region in which the dispersion is approximately linear. For linear dispersion about the resonant frequency we should have that $v_G(\omega) \simeq v_G(\omega_0)$. In Fig. 5 (b), (d) and (f) we show the corresponding scaled group velocity $\tilde{v}_G(\omega) = v_G(\omega)/v_G(\omega_0)$ for $n = 3, 5$ and 7 nanoparticles. For $n = 3$, one can see in Fig. 9 (a) that the nanoparticle array can provide a transfer channel giving an average fidelity of up to ~ 0.93 even when damping is present, although for large bandwidths σ the source and drain couplings g_{in} and g_{out} must be increased to values close to the limit of the weak coupling approximation, $|g_{\text{in,out}}/g_{np}^{\text{max}}| = 1$. Note that in these plots one cannot decrease the coupling g_{np} in order to reach $g_{\text{in,out}}$ values much larger than 1, as we have set $g_{np} = -0.1\omega_0$, unlike the ideal case where it could be modified. The reason for this restriction is that reducing the nanoparticle coupling g_{np} means the damping rates begin to dominate, lowering the maximum transmission and average fidelities further as a result.

For $n = 5$, one can see in Fig. 9 (c) that the maximum average fidelity attainable is ~ 0.89 ; no contour can be plotted for 0.9 or above, regardless of the bandwidth σ . For $n = 7$ and above, this situation then becomes gradually worse and one can see in Fig. 9 (e) that although the maximum average fidelity attainable is ~ 0.85 , the source and drain couplings need to be increased close to the weak coupling limit, in addition to the use of a narrow enough bandwidth.

The results obtained here indicate that only small-sized arrays with $n \lesssim 9$ are useful for the transmission of qubit states encoded into the number state degree of freedom. However, it may be the case that for particular applications, short-distance ($\lesssim \mu\text{m}$) communication is required at optical frequencies, making the use of a nanoparticle array quite beneficial. For example, the nanoparticle waveguide could be used as an enhanced mediator between emitter systems on a very small

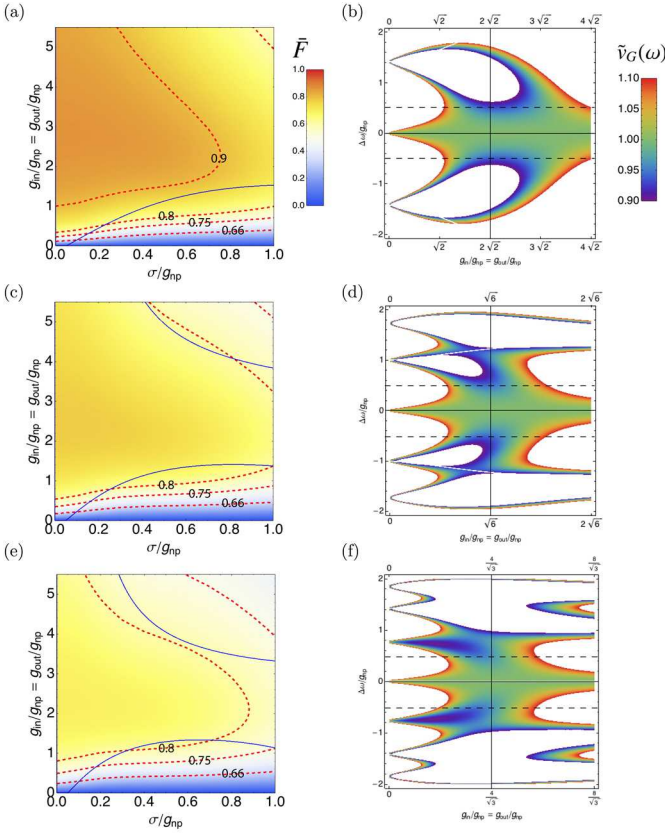


FIG. 9: Fidelity of quantum state transfer for a single qubit wavepacket under damping and scaled group velocity over a range of frequencies and couplings. **(a)**: Average fidelity \bar{F} for transferring a qubit wavepacket over $n = 3$ nanoparticles as the bandwidth (σ) and in/out couplings $g_{in} = g_{out}$ are modified. All parameters are scaled by g_{np} **(b)**: Scaled group velocity $\tilde{v}_G(\omega) = v_G(\omega)/v_G(\omega_0)$ as it deviates from that at the resonance frequency ω_0 for $n = 3$, showing the regions of approximate linear dispersion. **(c)**: Average fidelity for transferring a qubit wavepacket over $n = 5$ nanoparticles. **(d)**: Scaled group velocity $\tilde{v}_G(\omega)$ as it deviates from that at the resonance frequency ω_0 for $n = 5$. **(e)**: Average fidelity for transferring a qubit wavepacket over $n = 7$ nanoparticles. **(f)**: Scaled group velocity $\tilde{v}_G(\omega)$ as it deviates from that at the resonance frequency ω_0 for $n = 7$. In all group velocity plots, the region inside the dotted lines for $\Delta\omega$ corresponds to the frequency range σ shown in the average fidelity plots.

scale. On the other hand, other degrees of freedom for the LSP excitations, the embedding of emitter systems into the waveguides, novel types of metals with reduced damping rates and new schemes for achieving gain in plasmonic media may enable one to eventually counter the effects of loss highlighted here.

IV. SUMMARY

In this work we studied the use of an array of metallic nanoparticles as a channel for on-chip nanophotonic quantum communication. After introducing the model for the physical system in the quantum regime, the transfer of a quantum state

encoded in the form of a single-qubit wavepacket was studied under ideal conditions. The effects of loss in the metal were then included in order to put the investigation into a more practical setting and quantify the performance of realistic nanoparticle arrays as quantum channels. For this task we used the average fidelity for the state transfer. We found that only small-sized arrays are practically useful for the transmission of qubit states encoded into the number state degree of freedom. Our study highlights the benefits as well as the drawbacks associated with nanophotonic periodic quantum systems that use surface plasmons. We hope the techniques introduced in this work will contribute to the further study of plasmonic nanostructures for quantum control applications and probing nanoscale optical phenomena.

Acknowledgments

We thank Prof. M. S. Kim, Dr. S. K. Ozdemir and Prof. J. Takahara for discussions. We acknowledge funding from KRF and EPSRC.

APPENDIX A

Here we provide the analytical forms for the $\mathcal{T}(\omega)$'s for $n = 1, 2, 3, 5, 7$ and 9 nanoparticles respectively (no damping), where we have set $g_{out} = g_{in}$,

$$\begin{aligned} \mathcal{T}_1(\omega) &= \frac{g_{in}}{g_{in} - i(\omega - \omega_0)}, \\ \mathcal{T}_2(\omega) &= \frac{-4ig_{in}}{4g^2 + (g_{in} - 2i(\omega - \omega_0))^2}, \\ \mathcal{T}_3(\omega) &= \frac{-4g^2g_{in}}{(g_{in} - 2i(\omega - \omega_0))(4g^2 - (\omega - \omega_0)(ig_{in} + 2(\omega - \omega_0)))}, \\ \mathcal{T}_5(\omega) &= 4g^4g_{in}[(2g^2(g_{in} - 3i(\omega - \omega_0)) \\ &\quad - (g_{in} - 2i(\omega - \omega_0))(\omega - \omega_0)^2) \times \\ &\quad (2g^2 - (\omega - \omega_0)(ig_{in} + 2(\omega - \omega_0)))]^{-1}, \\ \mathcal{T}_7(\omega) &= -4g^6g_{in}[(g^2(g_{in} - 4i(\omega - \omega_0)) \\ &\quad - (g_{in} - 2i(\omega - \omega_0))(\omega - \omega_0)^2) \times \\ &\quad (4g^4 + (\omega - \omega_0)^3(ig_{in} + 2(\omega + \omega_0)) \\ &\quad - g^2(\omega - \omega_0)(3ig_{in} + 8(\omega + \omega_0)))]^{-1}, \end{aligned}$$

and

$$\begin{aligned} \mathcal{T}_9(\omega) &= 4g^8g_{in}[(2g^4(g_{in} - 5i(\omega - \omega_0)) \\ &\quad - 2g^2(2g_{in} - 5i(\omega - \omega_0))(\omega - \omega_0)^2) \\ &\quad + (g_{in} - 2i(\omega - \omega_0))(\omega - \omega_0)^4) \times \\ &\quad (2g^4 + (ig_{in} + 2(\omega + \omega_0))(\omega - \omega_0)^3 \\ &\quad + 2g^2(\omega - \omega_0)(ig_{in} + 3(\omega - \omega_0)))]^{-1}. \end{aligned}$$

APPENDIX B

Here we show how to obtain the output density matrix for the qubit state entering the drain nanowire. This is done in the

general case of damping (see Section III). To obtain the case of no loss, simply set $\mathcal{S}_i(\omega) = 0$, $\forall i$. Starting with the single qubit wavepacket in the input modes of the source nanowire

$$|\psi\rangle_s = \alpha |0\rangle_s + \beta \int d\omega \xi(\omega) \hat{s}_{\text{in}}^\dagger(\omega) |0\rangle_s. \quad (\text{B-1})$$

and making use of Eq. (29) of Section III, (equivalent to Eq. (20) of Section II, when $\mathcal{S}_i(\omega) = 0$, $\forall i$), substituting for $\hat{s}_{\text{in}}^\dagger(\omega)$ one obtains the state $\rho_{sda} = |\phi\rangle_{sda}\langle\phi|$ which describes the total state in the output modes of the *source-drain-array* system, where

$$|\phi\rangle_{sda} = \alpha |0\rangle_{sda} + \beta \int d\omega \xi(\omega) \left[\mathcal{R}(\omega) \hat{s}_{\text{out}}^\dagger(\omega) + \mathcal{T}(\omega) \hat{d}_{\text{out}}^\dagger(\omega) + \sum_{i=1}^n \mathcal{S}_i(\omega) \hat{A}_{\text{out},i}^\dagger(\omega) \right] |0\rangle_{sda} \quad (\text{B-2})$$

Removing the source modes from the description of the state ρ_{sda} is achieved mathematically by *tracing* them out to give

$$\rho_{da} = {}_s\langle 0 | \rho_{sda} | 0 \rangle_s + \int d\omega {}_s\langle 1_\omega | \rho_{sda} | 1_\omega \rangle_s. \quad (\text{B-3})$$

Tracing out the i array modes recursively in a similar way gives

$$\begin{aligned} \rho_d = & \left(|\alpha|^2 + |\beta|^2 \int d\omega |\xi(\omega)|^2 (1 - |\mathcal{T}(\omega)|^2) \right) |0\rangle_d \langle 0| \quad (\text{B-4}) \\ & + \alpha \beta^* \int d\omega \xi^*(\omega) \mathcal{T}^*(\omega) |0\rangle_d \langle 1_\omega| \\ & + \alpha^* \beta \int d\omega \xi(\omega) \mathcal{T}(\omega) |1_\omega\rangle_d \langle 0| \end{aligned}$$

$$+ |\beta|^2 \int d\omega \int d\omega' \xi(\omega) \xi^*(\omega') \mathcal{T}(\omega) \mathcal{T}^*(\omega') |1_\omega\rangle_d \langle 1_{\omega'}|.$$

APPENDIX C

Here we provide the analytical forms for the $\mathcal{T}(\omega)$'s for $n = 1, 2, 3, 5$ and 7 nanoparticles respectively with damping, where we have set $g_{\text{out}} = g_{\text{in}}$,

$$\mathcal{T}_1(\omega) = \frac{2g_{\text{in}}}{2g_{\text{in}} + \Gamma - 2i(\omega - \omega_0)},$$

$$\mathcal{T}_2(\omega) = \frac{-4igg_{\text{in}}}{4g^2 + (g_{\text{in}} + \Gamma - 2i(\omega - \omega_0))^2},$$

$$\mathcal{T}_3(\omega) = -8g^2 g_{\text{in}} [(g_{\text{in}} + \Gamma - 2i(\omega - \omega_0)) \times (8g^2 + (\Gamma - 2i(\omega - \omega_0))(g_{\text{in}} + \Gamma - 2i(\omega - \omega_0)))]^{-1},$$

$$\begin{aligned} \mathcal{T}_5(\omega) = & 32g^4 g_{\text{in}} [(4g^2 + (\Gamma + 2i(\omega - \omega_0))(g_{\text{in}} + \Gamma - 2i(\omega - \omega_0))) \\ & \times (4g^2 (2g_{\text{in}} + 3(\Gamma - 2i(\omega - \omega_0))) \\ & + (\Gamma - 2i(\omega - \omega_0))^2 (g_{\text{in}} + \Gamma - 2i(\omega - \omega_0)))]^{-1}, \end{aligned}$$

and

$$\begin{aligned} \mathcal{T}_7(\omega) = & -128g^6 g_{\text{in}} [((4g^2 (g_{\text{in}} + 2(\Gamma - 2i(\omega - \omega_0))) + \\ & (\Gamma - 2i(\omega - \omega_0))^2 (g_{\text{in}} + \Gamma - 2i(\omega - \omega_0))) \times \\ & (32g^4 + 4g^2 (3g_{\text{in}} + 4(\Gamma - 2i(\omega - \omega_0)))(\Gamma - \\ & 2i(\omega - \omega_0)) + (\Gamma - 2i(\omega - \omega_0))^3 \times \\ & (g_{\text{in}} + \Gamma - 2i(\omega - \omega_0)))]^{-1}. \end{aligned}$$

-
- [1] E. Altewischer, M. P. van Exter and J. P. Woerdman, *Nature* **418**, 304 (2002).
- [2] S. Fasel, F. Robin, E. Moreno, D. Erni, N. Gisin, and H. Zbinden, *Phys. Rev. Lett.* **94**, 110501 (2005); S. Fasel, M. Halder, N. Gisin and H. Zbinden, *New J. Phys.* **8**, 13 (2006).
- [3] A. Huck, S. Smolka, P. Lodahl, A. S. Sorensen, A. Boltasseva, J. Janousek and U. L. Andersen, *Phys. Rev. Lett.* **102**, 246802 (2009).
- [4] A. Gonzalez-Tudela, D. Martin-Cano, E. Moreno, L. Martin-Moreno, C. Tejedor, and F. J. Garcia-Vidal, *Phys. Rev. Lett.* **106**, 020501 (2011).
- [5] J. L. van Velsen, J. Tworzydło and C. W. J. Beenakker, *Phys. Rev. A* **68** 043807 (2003); X.-F. Ren, G.-P. Guo, Y.-F. Huang, Z.-W. Wang, G.-C. Guo, *Opt. Lett.* **31**, 2792 (2006); A. Kamli, S. A. Moiseev and B. C. Sanders, *Phys. Rev. Lett.* **101**, 263601 (2008).
- [6] M. S. Tame, C. Lee, J. Lee, D. Ballester, M. Paternostro, A. V. Zayats and M. S. Kim, *Phys. Rev. Lett.* **101**, 190504 (2008).
- [7] D. Ballester, M. S. Tame, C. Lee, J. Lee and M. S. Kim, *Phys. Rev. A* **79**, 053845 (2009).
- [8] D. Ballester, M. S. Tame and M. S. Kim, *Phys. Rev. A* **82**, 012325 (2010).
- [9] A. L. Falk, F. H. L. Koppens, C. L. Yu, K. Kang, N. de Leon Snapp, A. V. Akimov, M.-H. Jo, M. D. Lukin, H. Park, *Nature Phys.* **5**, 475 (2009).
- [10] R. W. Heeres *et al.*, *Nano Letters* **10**, 661 (2011).
- [11] A. Cuche *et al.*, *Nano Letters* **10**, 4566 (2011).
- [12] D. E. Chang, A. S. Sorensen, E. A. Demler, M. D. Lukin, *Nature Phys.* **3**, 807 (2007).
- [13] D. E. Chang, A. S. Sorensen, P. R. Hemmer and M. D. Lukin, *Phys. Rev. Lett.* **97**, 053002 (2006); A. V. Akimov, A. Mukherjee, C. L. Yu, D. E. Chang, A. S. Zibrov, P. R. Hemmer, H. Park, M. D. Lukin, *Nature* **450**, 402 (2007).
- [14] R. Kolesov, B. Grotz, G. Balasubramanian, R. J. Stöhr, A. A. L. Nicolet, P. R. Hemmer, F. Jelezko and J. Wrachtrup, *Nature Phys.* **5**, 470 (2009).
- [15] D. Dzsojtjan, A. S. Sørensen and M. Fleischhauer, *Phys. Rev. B* **82**, 075427 (2010); D. Dzsojtjan, J. Kaestel, M. Fleischhauer, arXiv:1105.1018 (2011).
- [16] Y. Fedutik, V. V. Temnov, O. Schops, U. Woggon, and M. V. Artemyev, *Phys. Rev. Lett.* **99**, 136802 (2007).
- [17] P. Kolchin, R. F. Oulton and X. Zhang, *Phys. Rev. Lett.* **106**, 113601 (2011).
- [18] D. E. Chang, A. S. Sørensen, P. R. Hemmer and M. D. Lukin, *Phys. Rev. B* **76**, 035420 (2007).
- [19] D. J. Bergman and M. I. Stockman, *Phys. Rev. Lett.* **90**, 027402 (2003).
- [20] J. Takahara, S. Yamagisha, H. Taki, A. Morimoto and T. Kobayashi, *Opt. Lett.* **22**, 475 (1997).
- [21] D. K. Gramotnev and S. I. Bozhevolnyi, *Nature Photonics* **4**, 83

- (2010).
- [22] A. V. Zayats, I. I. Smolyaninov and A. A. Maradudin, *Phys. Rep.* **408**, 131 (2005).
- [23] W. L. Barnes, A. Dereux and T. W. Ebbesen, *Nature* **424**, 824 (2003).
- [24] S. A. Maier, *IEEE J. Sel. Top. Quant. Elec.* **12**, 1214 (2006); S. A. Maier *ibid.* **12**, 1671 (2006).
- [25] J. B. Pendry, L. Martin-Moreno and F. J. Garcia-Vidal, *Science*, **305**, 847 (2004); A. P. Hibbins, B. R. Evans and J. R. Sambles, *Science* **308**, 670 (2005); A. P. Hibbins, E. Hendry, M. J. Lockyear and J. R. Sambles, *Opt. Express* **16**, 20441 (2008); E. Hendry, A. P. Hibbins and J. R. Sambles, *Phys. Rev. B* **78**, 235426 (2008); S. Collin, C. Sauvan, C. Billaudeau, F. Pardo, J. C. Rodier, J. L. Pelouard and P. Lalanne, *Phys. Rev. B* **79**, 165405 (2009).
- [26] D. Wasserman, E. A. Shaner and J. G. Cederberg, *Appl. Phys. Lett.* **90**, 191102 (2007); E. A. Shaner, J. G. Cederberg and D. Wasserman, *Appl. Phys. Lett.* **91**, 181110 (2007).
- [27] M. Quinten, A. Leitner, J. R. Krenn, and F. R. Aussenegg, *Opt. Lett.* **23**, 1331 (1998).
- [28] S. A. Maier, P. G. Kik, H. A. Atwater, S. Meltzer, E. Harel, B. E. Koel and A. A. G. Requicha, *Nature Materials* **2**, 229 - 232 (2003).
- [29] M. L. Brongersma, J. W. Hartman and H. A. Atwater, *Phys. Rev. B* **62**, R16356 (2000).
- [30] J. R. Krenn, A. Dereux, J. C. Weeber, E. Bourillot, Y. Lacroute, J. P. Goudonnet, G. Schider, W. Gotschy, A. Leitner, F. R. Aussenegg, and C. Girard, *Phys. Rev. Lett.* **82**, 2590 (1999).
- [31] J. R. Krenn, M. Salerno, N. Felidj, B. Lamprecht, G. Schider, A. Leitner, F. R. Aussenegg, J. C. Weeber, A. Dereux, and J. P. Goudonnet, *J. Microscopy* **202**, 122 (2001).
- [32] S. A. Maier, *Plasmonics: Fundamentals and Applications*, (Springer, New York, 2007).
- [33] B. Yurke and W. Kuang, *Phys. Rev. A* **81**, 033814 (2010).
- [34] Y. Kubota and K. Nobusada, *J. Chem. Phys.* **134**, 044108 (2011).
- [35] R. Baer, K. Lopata and D. Neuhauser, *J. Chem. Phys.* **126**, 014705 (2007).
- [36] S. Y. Park and D. Stroud, *Phys. Rev. B* **69**, 125418 (2004).
- [37] J. M. Elson and R. H. Ritchie, *Phys. Rev. B* **4**, 4129 (1971); J. Nkoma, R. Loudon and D. R. Tilley, *J. Phys. C: Solid State Phys.* **7**, 3547 (1974); M. S. Tomaš and M. Šunjić, *Phys. Rev. B* **12** 5363 (1975); Y. O. Nakamura, *Prog. Theor. Phys.* **70**, 908 (1983).
- [38] W. Greiner, *Classical Electrodynamics*, (Springer-Verlag, New York, 1996), p. 429.
- [39] E. D. Palik, *Handbook of Optical Constants of Solids* (Academic, San Diego, 1998).
- [40] J. Zuloaga, E. Prodan and P. Nordlander, *Nano Lett.* **9**, 887 (2009).
- [41] R. Loudon, *The Quantum Theory of Light*, 3rd Ed., Oxford University Press, Oxford (2000).
- [42] C. Ropers *et al.*, *Nano Lett.* **7**, 2784 (2007).
- [43] D. E. Chang, J. D. Thompson, H. Park, V. Vuletic, A. S. Zibrov, P. Zoller and M. D. Lukin, *Phys. Rev. Lett.* **103**, 123004 (2009).
- [44] N. A. Issa and R. Guckenberger, *Opt. Express* **15**, 12131 (2007).
- [45] M. J. Collett and C. W. Gardiner, *Phys. Rev. A* **30**, 1386 (1984).
- [46] D. F. Walls and G. J. Milburn, *Quantum Optics* (Springer, Berlin, 1994).
- [47] M. Agio, arXiv:1111.1302 (2011).
- [48] M. I. Stockman, *Phys. Rev. Lett.* **93**, 137404 (2004).
- [49] F. Ciccarello, *Phys. Rev. A* **83**, 043802 (2011).
- [50] A. Yariv, Y. Xu, R. K. Lee, A. Scherer, *Opt. Lett.* **24**, 711 (1999); M. Bayindir, B. Temelkuran and E. Ozbay, *Phys. Rev. Lett.* **84**, 2140 (2000); M. Notomi, E. Kuramochi and T. Tanabe, *Nature Photonics* **2**, 741 (2008).
- [51] P. B. Johnson and R. W. Christy, *Phys. Rev. B* **6**, 4370 (1972).
- [52] M. Horodecki, P. Horodecki and R. Horodecki, *Phys. Rev. A* **60**, 1888 (1999).
- [53] N. A. Januts, K. S. Baghdasaryan, Kh. V. Nerkararyan and B. Hecht, *Opt. Comm.* **253**, 118 (2005); W. Ding, S. R. Andrews and S. A. Maier, *Phys. Rev. A* **75**, 063822 (2007).